PHYSICAL REVIEW D **83,** 095021 (2011)

Two-singlet model for light cold dark matter

Abdessamad Abada,[1,*] Djamal Ghaffor,[2,†] and Salah Nasri[3,‡]

[1]*Laboratoire de Physique des Particules et Physique Statistique, Ecole Normale Supérieure, BP 92 Vieux Kouba, 16050 Alger, Algeria*
[2]*Laboratoire de Physique Théorique d'Oran, Es-Senia University, 31000 Oran, Algeria*
[3]*Physics Department, UAE University, POB 17551, Al Ain, United Arab Emirates*

(Received 11 January 2011; published 26 May 2011)

We extend the standard model by adding two gauge-singlet $\mathbb{Z}_2$-symmetric scalar fields that interact with visible matter only through the Higgs particle. One is a stable dark matter WIMP, and the other one undergoes a spontaneous breaking of the symmetry that opens new channels for the dark matter annihilation, hence lowering the mass of the WIMP. We study the effects of the observed dark matter relic abundance on the WIMP annihilation cross section and find that in most regions of the parameters' space, light dark matter is viable. We also compare the elastic-scattering cross section of our dark matter candidate off a nucleus with existing (CDMSII and XENON100) and projected (SuperCDMS and XENON1T) experimental exclusion bounds. We find that most of the allowed mass range for light dark matter will be probed by the projected sensitivity of the XENON1T experiment.

DOI: 10.1103/PhysRevD.83.095021 PACS numbers: 95.35.+d, 11.30.Qc, 12.15.−y, 98.80.−k

I. INTRODUCTION

Cosmology tells us that about 25% of the total mass density in the Universe is dark matter that cannot be accounted for by conventional baryons [1]. Alongside observation, intense theoretical efforts are made in order to elucidate the nature and properties of this unknown form of matter. In this context, electrically neutral and colorless weakly interacting massive particles (WIMPs) form an attractive scenario. Their broad properties are: masses in the range of one to a few hundred GeV, coupling constants in the milliweak scale and lifetimes longer than the age of the Universe.

Recent data from the direct-detection experiments DAMA/LIBRA [2] and CoGeNT [3], and the recent analysis of the data from the Fermi Gamma Ray Space Telescope [4], if interpreted as a signal for dark matter, require light WIMPs in the range of 5 to 10 GeV [5]. Also, galactic substructure requires still lighter dark matter masses [6,7]. In this regard, it is useful to note in passing that the XENON100 collaboration has provided serious constraints on the region of interest to DAMA/LIBRA and CoGeNT [8], assuming a constant extrapolation of the liquid xenon scintillation response for nuclear recoils below 5 keV, a claim disputed in [9]. Also, most recently, the CDMS collaboration has released the analysis of their low-energy threshold data [10] which seems to exclude the parameter space for dark matter interpretation of DAMA/LIBRA and CoGeNT results, assuming a standard halo dark-matter model with an escape velocity $v_{\rm esc} = 544$ km/s and neglecting the effect of ion channeling [11]. However, with a highly anisotropic velocity distribution, it may be possible to reconcile the CoGeNT and DAMA/LIBRA results with the current exclusion limits from CDMS and XENON [12]; see also comments on p. 6 in [13] about the possibility of shifting the exclusion contour in [10] above the CoGeNT signal region. In addition, CRESST, another direct detection experiment at Gran Sasso, which uses $CaWO_4$ as target material, reported in talks at the IDM 2010 and WONDER 2010 workshops an excess of events in their oxygen band instead of tungsten band. If this signal is not due to neutron background, a possible interpretation could be the elastic scattering of a light WIMP depositing a detectable recoil energy on the lightest nuclei (oxygen) in the detector [14]. While this result has to await confirmation from the CRESST collaboration, it is clear that it is important as well as interesting to study dark matter with light masses.

The most popular candidate for dark matter is the neutralino, a neutral R-odd supersymmetric particle. Indeed, neutralinos are only produced or destroyed in pairs, thus rendering the lightest SUSY particle stable [15]. In the minimal version of the supersymmetric extension of the standard model, neutralinos χ_1^0 are linear combinations of the fermionic partners of the neutral electroweak gauge bosons (gauginos) and the neutral Higgs bosons (higgsinos). They can annihilate through a t-channel sfermion exchange into standard model fermions, or via a t-channel chargino-mediated process into W^+W^-, or through an s-channel pseudoscalar Higgs exchange into fermion pairs. They can also undergo elastic scattering with nuclei through mainly a scalar Higgs exchange [16].

However, having a neutralino as a *light* dark matter candidate can be challenging in many ways. For example, in mSUGRA, the constraint from WMAP and the bound on the pseudoscalar Higgs mass from LEP give the limitation $m_{\chi_1^0} \geq 50$ GeV [17]. If one allows the gaugino masses M_1 and M_2 to be free parameters whereas the gluino mass

*a.abada@uaeu.ac.ae
†dghaffor@mail-enset.dz
‡snasri@uaeu.ac.ae

satisfies the universal condition at some grand unification scale, that is, $M_3 = 3M_2$, then the lightest SUSY particle should be heavier than about 28 GeV [18]; see also [19]. A similar analysis is done in [20] with the gluino mass taken as a free parameter, and it is concluded that the lower limit on the neutralino mass can vary between about 7 GeV and 12 GeV, depending on the gluino mass and the degeneracy of the squarks. Also, in the extension of the MSSM with an extra singlet chiral superfield (NMSSM), a model with 11 input parameters, it is found that a neutralino with a mass of the order of a few GeV is possible with a higher likelihood peaked around 15 GeV [18].

Therefore, with the aim of describing dark matter as light as, say 1 GeV and smaller, and with no clear clue yet as to what the internal structure of the WIMP is, if any, a pedestrian approach can be attractive. In this logic, the simplest of models is to extend the standard model by adding a real scalar field, the dark matter, a standard model gauge singlet that interacts with visible particles via the Higgs field only. To ensure stability, it is endowed with a discrete $\mathbb{Z}_2$ symmetry that does not break spontaneously. Such a model can be seen as a low-energy remnant of some higher-energy physics waiting to be understood. In this cosmological setting, such an extension has first been proposed in [21] and further studied in [22] where the unbroken $\mathbb{Z}_2$ symmetry is extended to a global U(1) symmetry. A more extensive exploration of the model and its implications was done in [23], specific implications on Higgs detection and LHC physics discussed in [24] and one-loop vacuum stability looked into and perturbativity bounds obtained in [25]. The work of [26] considers also this minimal extension and uses constraints from the experiments XENON10 [27] and CDMSII [28] to exclude dark matter masses smaller than 50, 70 and 75 GeV for Higgs masses equal to 120, 200 and 350 GeV, respectively. Furthermore, it was recently shown that the Fermi-LAT data on the isotropic diffuse gamma-ray emission can potentially excludes the one-singlet dark-matter model for masses as low as 6 GeV, assuming a NFW profile for the dark matter distribution [29].

In order to allow for light dark matter in this bottom-up approach, it is therefore necessary to go beyond the minimal one-real-scalar extension of the standard model. The natural next step is to add another real scalar field, endowed with a $\mathbb{Z}_2$ symmetry too, but one which is spontaneously broken so that new channels for dark matter annihilation are opened, increasing this way the annihilation cross section, hence allowing smaller masses. This auxiliary field must also be a standard model gauge singlet. The aim of this work is to introduce this extension.

After this brief introductory motivation, we present the model in the next section. We perform the spontaneous breaking of the electroweak and the additional $\mathbb{Z}_2$ symmetries in the usual way. We clarify the physical modes as well as the physical parameters. There is mixing between the physical new scalar field and the Higgs, and this is one of the quantities parametrizing the subsequent physics. In Sec. III, we impose the constraint from the known dark matter relic density on the dark matter annihilation cross section and study its effects. Of course, as we will see, the parameter space is quite large, and so it is not realistic to hope to cover all of it in one single work of acceptable size. Representative values have to be selected and the behavior of the model, as well as its capabilities, are described. Though our main interest in this study is light dark matter, we allow the mass range to be 0.1 GeV–100 GeV. We find that the model is rich enough to bear dark matter in most of it, including the very light sector. In Sec. IV, we determine the total cross section $\sigma_{\rm det}$ for nonrelativistic elastic scattering of dark matter off a nucleon target and compare it to the current direct-detection experimental bounds and projected sensitivity. For this, we choose the results of CDMSII and XENON100, and the projections of SuperCDMS [30] and XENON1T [31]. Here, too, we cannot cover all of the parameter space nor are we going to give a detailed account of the behavior of $\sigma_{\rm det}$ as a function of the dark matter mass, but general patterns are mentioned. The last section is devoted to some concluding remarks. Note that, as a rule, we have avoided in this first study narrowing the choice of parameters using particle phenomenology. Of course, such phenomenological constraints have to be addressed ultimately and this is left to a forthcoming investigation [32], contenting ourselves in the present work with a limited set of remarks mentioned in this last section. Finally, we have gathered in the Appendix the partial results regarding the calculation of the dark matter annihilation cross section.

II. A TWO-SINGLET MODEL FOR DARK MATTER

We extend thestandard model by adding two real, spinless and $\mathbb{Z}_2$-symmetric fields: the dark matter field S_0 for which the $\mathbb{Z}_2$ symmetry is unbroken, and an auxiliary field χ_1 for which it is spontaneously broken. Both fields are standard model gauge singlets and hence can interact with "visible" particles only via the Higgs doublet H. This latter is taken in the unitary gauge such that $H^\dagger = 1/\sqrt{2}(0h')$, where h' is a real scalar. We assume all processes calculable in perturbation theory. The potential function that includes S_0, h', and χ_1 is written as follows:

$$U = \frac{\tilde{m}_0^2}{2}S_0^2 - \frac{\mu^2}{2}h'^2 - \frac{\mu_1^2}{2}\chi_1^2 + \frac{\eta_0}{24}S_0^4 + \frac{\lambda}{24}h'^4 + \frac{\eta_1}{24}\chi_1^4 + \frac{\lambda_0}{4}S_0^2h'^2 + \frac{\eta_{01}}{4}S_0^2\chi_1^2 + \frac{\lambda_1}{4}h'^2\chi_1^2, \quad (2.1)$$

where $\tilde{m}_0^2$, μ^2, and μ_1^2 and all the coupling constants are real positive numbers. In the standard model scenario, electroweak spontaneous symmetry breaking occurs for the Higgs field, which then oscillates around the vacuum expectation value $v = 246$ GeV [33]. The field χ_1 will oscillate around the vacuum expectation value $v_1 > 0$.

Both v and v_1 are related to the parameters of the theory by the two relations:

$$v^2 = 6\frac{\mu^2\eta_1 - 6\mu_1^2\lambda_1}{\lambda\eta_1 - 36\lambda_1^2}; \quad v_1^2 = 6\frac{\mu_1^2\lambda - 6\mu^2\lambda_1}{\lambda\eta_1 - 36\lambda_1^2}. \tag{2.2}$$

It is assumed that the self-coupling constants are sufficiently larger than the mutual ones.

Writing $h' = v + \tilde{h}$ and $\chi_1 = v_1 + \tilde{S}_1$, the potential function becomes, up to an irrelevant zero-field energy:

$$U = U_{\text{quad}} + U_{\text{cub}} + U_{\text{quar}}, \tag{2.3}$$

where the mass-squared (quadratic) terms are gathered in U_{quad}, the cubic interactions in U_{cub} and the quartic ones in U_{quar}. The quadratic terms are given by

$$U_{\text{quad}} = \frac{1}{2}m_0^2S_0^2 + \frac{1}{2}M_h^2\tilde{h}^2 + \frac{1}{2}M_1^2\tilde{S}_1^2 + M_{1h}^2\tilde{h}\tilde{S}_1, \tag{2.4}$$

where the mass-squared coefficients are related to the original parameters of the theory by the following relations:

$$\begin{aligned} m_0^2 &= \tilde{m}_0^2 + \frac{\lambda_0}{2}v^2 + \frac{\eta_{01}}{2}v_1^2; \qquad M_h^2 = -\mu^2 + \frac{\lambda}{2}v^2 + \frac{\lambda_1}{2}v_1^2; \\ M_1^2 &= -\mu_1^2 + \frac{\lambda_1}{2}v^2 + \frac{\eta_1}{2}v_1^2; \quad M_{1h}^2 = \lambda_1 v v_1. \end{aligned} \tag{2.5}$$

Replacing the vacuum expectation values v and v_1 by their respective expressions (2.2) will not add clarity. In this field basis, the mass-squared matrix is not diagonal: there is mixing between the fields $\tilde{h}$ and $\tilde{S}_1$. Denoting the physical mass-squared field eigenmodes by h and S_1, we rewrite

$$U_{\text{quad}} = \frac{1}{2}m_0^2S_0^2 + \frac{1}{2}m_h^2h^2 + \frac{1}{2}m_1^2S_1^2, \tag{2.6}$$

where the physical fields are related to the mixed ones by a 2×2 rotation:

$$\begin{pmatrix} h \\ S_1 \end{pmatrix} = \begin{pmatrix} \cos\theta & \sin\theta \\ -\sin\theta & \cos\theta \end{pmatrix}\begin{pmatrix} \tilde{h} \\ \tilde{S}_1 \end{pmatrix}. \tag{2.7}$$

Here, θ is the mixing angle, related to the original mass-squared parameters by the relation

$$\tan 2\theta = \frac{2M_{1h}^2}{M_1^2 - M_h^2}, \tag{2.8}$$

and the physical masses in (2.6) by the two relations

$$\begin{aligned} m_h^2 &= \frac{1}{2}\Big[M_h^2 + M_1^2 + \varepsilon(M_h^2 - M_1^2) \\ &\quad \times \sqrt{(M_h^2 - M_1^2)^2 + 4M_{1h}^4}\Big]; \\ m_1^2 &= \frac{1}{2}\Big[M_h^2 + M_1^2 - \varepsilon(M_h^2 - M_1^2) \\ &\quad \times \sqrt{(M_h^2 - M_1^2)^2 + 4M_{1h}^4}\Big], \end{aligned} \tag{2.9}$$

where ε is the sign function.

Written now directly in terms of the physical fields, the cubic interaction terms are expressed as follows:

$$\begin{aligned} U_{\text{cub}} &= \frac{\lambda_0^{(3)}}{2}S_0^2h + \frac{\eta_{01}^{(3)}}{2}S_0^2S_1 + \frac{\lambda^{(3)}}{6}h^3 + \frac{\eta_1^{(3)}}{6}S_1^3 \\ &\quad + \frac{\lambda_1^{(3)}}{2}h^2S_1 + \frac{\lambda_2^{(3)}}{2}hS_1^2, \end{aligned} \tag{2.10}$$

where the cubic physical coupling constants are related to the original parameters via the following relations:

$$\begin{aligned} \lambda_0^{(3)} &= \lambda_0 v\cos\theta + \eta_{01}v_1\sin\theta, \\ \eta_{01}^{(3)} &= \eta_{01}v_1\cos\theta - \lambda_0 v\sin\theta; \\ \lambda^{(3)} &= \lambda v\cos^3\theta + \frac{3}{2}\lambda_1\sin 2\theta(v_1\cos\theta + v\sin\theta) \\ &\quad + \eta_1 v_1\sin^3\theta; \\ \eta_1^{(3)} &= \eta_1 v_1\cos^3\theta - \frac{3}{2}\lambda_1\sin 2\theta(v\cos\theta - v_1\sin\theta) \\ &\quad - \lambda v\sin^3\theta; \\ \lambda_1^{(3)} &= \lambda_1 v_1\cos^3\theta + \frac{1}{2}\sin 2\theta[(2\lambda_1 - \lambda)v\cos\theta \\ &\quad - (2\lambda_1 - \eta_1)v_1\sin\theta] - \lambda_1 v\sin^3\theta; \\ \lambda_2^{(3)} &= \lambda_1 v\cos^3\theta - \frac{1}{2}\sin 2\theta[(2\lambda_1 - \eta_1)v_1\cos\theta \\ &\quad + (2\lambda_1 - \lambda)v\sin\theta] + \lambda_1 v_1\sin^3\theta. \end{aligned} \tag{2.11}$$

Also, in terms of the physical fields, the quartic interactions are given by

$$\begin{aligned} U_{\text{quar}} &= \frac{\eta_0}{24}S_0^4 + \frac{\lambda^{(4)}}{24}h^4 + \frac{\eta_1^{(4)}}{24}S_1^4 + \frac{\lambda_0^{(4)}}{4}S_0^2h^2 + \frac{\eta_{01}^{(4)}}{4}S_0^2S_1^2 \\ &\quad + \frac{\lambda_{01}^{(4)}}{2}S_0^2hS_1 + \frac{\lambda_1^{(4)}}{6}h^3S_1 + \frac{\lambda_2^{(4)}}{4}h^2S_1^2 + \frac{\lambda_3^{(4)}}{6}hS_1^3, \end{aligned} \tag{2.12}$$

where the physical quartic coupling constants are written in terms of the original parameters of the theory as follows:

$$
\begin{aligned}
\lambda^{(4)} &= \lambda\cos^4\theta + \frac{3}{2}\lambda_1\sin^2 2\theta + \eta_1\sin^4\theta,\\
\eta_1^{(4)} &= \eta_1\cos^4\theta + \frac{3}{2}\lambda_1\sin^2 2\theta + \lambda\sin^4\theta;\\
\lambda_0^{(4)} &= \lambda_0\cos^2\theta + \eta_{01}\sin^2\theta,\\
\eta_{01}^{(4)} &= \eta_{01}\cos^2\theta + \lambda_0\sin^2\theta;\\
\lambda_{01}^{(4)} &= \frac{1}{2}(\eta_{01} - \lambda_0)\sin 2\theta,\\
\lambda_1^{(4)} &= \frac{1}{2}[(3\lambda_1 - \lambda)\cos^2\theta - (3\lambda_1 - \eta_1)\sin^2\theta]\sin 2\theta;\\
\lambda_2^{(4)} &= \lambda_1\cos^2 2\theta - \frac{1}{4}(2\lambda_1 - \eta_1 - \lambda)\sin^2 2\theta;\\
\lambda_3^{(4)} &= \frac{1}{2}[(\eta_1 - 3\lambda_1)\cos^2\theta - (\lambda - 3\lambda_1)\sin^2\theta]\sin 2\theta.
\end{aligned}
\tag{2.13}
$$

Finally, after spontaneous breaking of the electroweak and $\mathbb{Z}_2$ symmetries, the part of the standard model Lagrangian that is relevant to dark matter annihilation is written, in terms of the physical fields h and S_1, as follows:

$$
\begin{aligned}
U_{\rm SM} = &\sum_f(\lambda_{hf}h\bar{f}f + \lambda_{1f}S_1\bar{f}f) + \lambda_{hw}^{(3)}hW_\mu^- W^{+\mu}\\
&+ \lambda_{1w}^{(3)}S_1W_\mu^- W^{+\mu} + \lambda_{hz}^{(3)}h(Z_\mu)^2 + \lambda_{1z}^{(3)}S_1(Z_\mu)^2\\
&+ \lambda_{hw}^{(4)}h^2W_\mu^- W^{+\mu} + \lambda_{1w}^{(4)}S_1^2W_\mu^- W^{+\mu}\\
&+ \lambda_{h1w}hS_1W_\mu^- W^{+\mu} + \lambda_{hz}^{(4)}h^2(Z_\mu)^2\\
&+ \lambda_{1z}^{(4)}S_1^2(Z_\mu)^2 + \lambda_{h1z}hS_1(Z_\mu)^2.
\end{aligned}
\tag{2.14}
$$

The quantities m_f, m_w, and m_z are the masses of the fermion f, the W, and the Z gauge bosons, respectively, and the above coupling constants are given by the following relations:

$$
\begin{aligned}
\lambda_{hf} &= -\frac{m_f}{v}\cos\theta; & \lambda_{1f} &= \frac{m_f}{v}\sin\theta;\\
\lambda_{hw}^{(3)} &= 2\frac{m_w^2}{v}\cos\theta; & \lambda_{1w}^{(3)} &= -2\frac{m_w^2}{v}\sin\theta;\\
\lambda_{hz}^{(3)} &= \frac{m_z^2}{v}\cos\theta; & \lambda_{1z}^{(3)} &= -\frac{m_z^2}{v}\sin\theta;\\
\lambda_{hw}^{(4)} &= \frac{m_w^2}{v^2}\cos^2\theta; & \lambda_{1w}^{(4)} &= \frac{m_w^2}{v^2}\sin^2\theta;\\
\lambda_{h1w} &= -\frac{m_w^2}{v^2}\sin 2\theta; & \lambda_{hz}^{(4)} &= \frac{m_z^2}{2v^2}\cos^2\theta;\\
\lambda_{1z}^{(4)} &= \frac{m_z^2}{2v^2}\sin^2\theta; & \lambda_{h1z} &= -\frac{m_z^2}{2v^2}\sin 2\theta.
\end{aligned}
\tag{2.15}
$$

III. RELIC DENSITY, MUTUAL COUPLINGS AND PERTURBATIVITY

The original theory (2.1) has nine parameters: three mass parameters $(\tilde{m}_0, \mu, \mu_1)$, three self-coupling constants $(\eta_0, \lambda, \eta_1)$ and three mutual coupling constants $(\lambda_0, \eta_{01}, \lambda_1)$. Perturbativity is assumed, hence all these original coupling constants are small. The dark matter self-coupling constant η_0 does not enter the calculations of the lowest-order processes of this work [34], so effectively we are left with eight parameters. The spontaneous breaking of the electroweak and $\mathbb{Z}_2$ symmetries for the Higgs and χ_1 fields, respectively, introduces the two vacuum expectation values v and v_1 given to lowest order in (2.2). The value of v is fixed experimentally to be 246 GeV, and for the present work we fix the value of v_1 at the order of the electroweak scale, say 100 GeV. Hence we are left with six parameters. Four of these are chosen to be the three physical masses m_0 (dark matter), m_1 (S_1 field) and m_h (Higgs), plus the mixing angle θ between S_1 and h. We will fix the Higgs mass to $m_h = 138$ GeV and give, in this section, the mixing angle θ the two values 10° (small) and 40° (larger). The two last parameters we choose are the two physical mutual coupling constants $\lambda_0^{(4)}$ (dark matter—Higgs) and $\eta_{01}^{(4)}$ (dark matter—S_1 particle), see (2.12).

In the framework of the thermal dynamics of the Universe within the standard cosmological model [35], the WIMP relic density is related to its annihilation rate by the familiar relations:

$$
\begin{aligned}
\Omega_D\bar{h}^2 &\simeq \frac{1.07\times 10^9 x_f}{\sqrt{g_*}m_{\rm Pl}\langle v_{12}\sigma_{\rm ann}\rangle{\rm GeV}};\\
x_f &\simeq \ln\frac{0.038 m_{\rm Pl}m_0\langle v_{12}\sigma_{\rm ann}\rangle}{\sqrt{g_* x_f}}.
\end{aligned}
\tag{3.1}
$$

The notation is as follows: the quantity $\bar{h}$ is the Hubble constant in units of 100 km $\times$ s^{-1} $\times$ Mpc^{-1}, the quantity $m_{\rm Pl} = 1.22\times 10^{19}$ GeV the Planck mass, m_0 the dark matter mass, $x_f = m_0/T_f$ the ratio of the dark matter mass to the freeze-out temperature T_f and g_* the number of relativistic degrees of freedom with mass less than T_f. The quantity $\langle v_{12}\sigma_{\rm ann}\rangle$ is the thermally averaged annihilation cross section of a pair of two dark matter particles multiplied by their relative speed in the center-of-mass reference frame. Solving (3.1) with the current value for the dark matter relic density $\Omega_D\bar{h}^2 = 0.1123 \pm 0.0035$ [36] gives

$$
\langle v_{12}\sigma_{\rm ann}\rangle \simeq (1.9 \pm 0.2)\times 10^{-9}\ {\rm GeV}^{-2},
\tag{3.2}
$$

for a range of dark matter masses between roughly 10 GeV to 100 GeV and x_f between 19.2 and 21.6, with about 0.4 thickness [37].

The value in (3.2) for the dark matter annihilation cross-section translates into a relation between the parameters of a given theory entering the calculated expression of $\langle v_{12}\sigma_{\rm ann}\rangle$, hence imposing a constraint on these parameters which will limit the intervals of possible dark matter masses. This constraint can be exploited to examine aspects of the theory like perturbativity, while at the same time reducing the number of parameters by one.

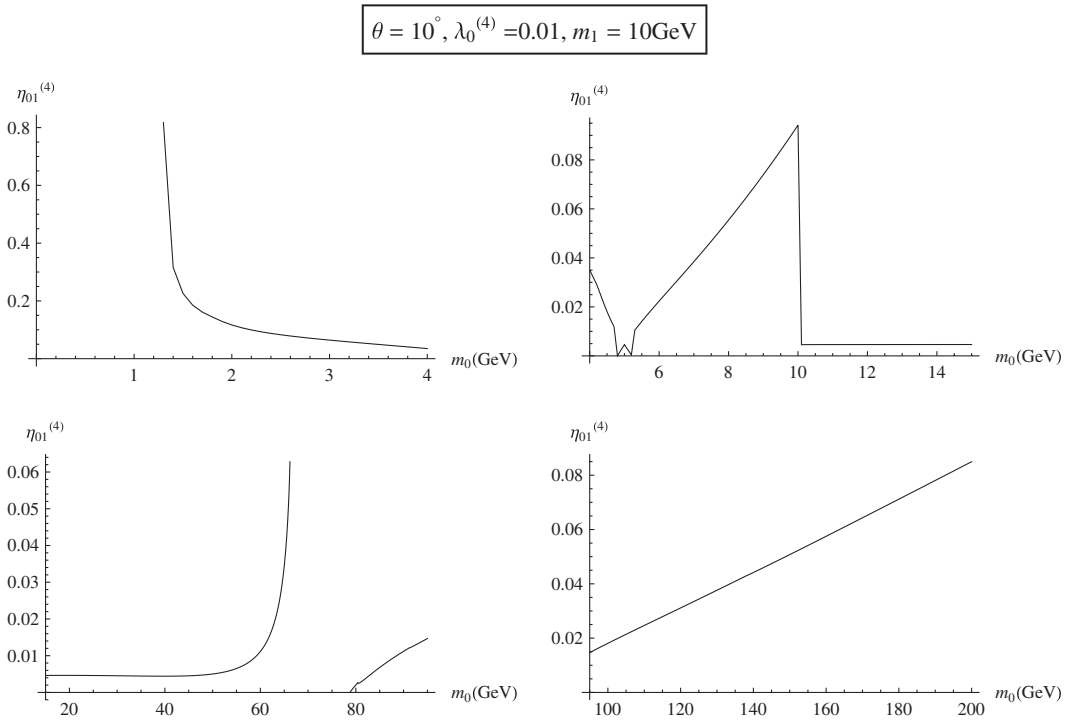

FIG. 1. $\eta_{01}^{(4)}$ vs m_0 for small m_1, small mixing and very small WIMP-Higgs coupling.

For example, in our model, we can obtain via (3.2) the mutual coupling constant $\eta_{01}^{(4)}$ for given values of $\lambda_0^{(4)}$, study its behavior as a function of m_0 and tell which dark-matter mass regions are consistent with perturbativity. Note that once the two mutual coupling constants $\lambda_0^{(4)}$ and $\eta_{01}^{(4)}$ are perturbative, all the other physical coupling constants will be. In the study of this section, we choose the values $\lambda_0^{(4)} = 0.01$ (very weak), 0.2 (weak), and 1 (large). We also let the two masses m_0 and m_1 stretch from 0.1 GeV to 120 GeV, occasionally m_0 to 200 GeV. Finally, note that we do not incorporate the uncertainty in (3.2) when imposing the relic-densityconstraint, something that is sufficient in view of the descriptive nature of this work.

The dark matter annihilation cross sections (times the relative speed) through all possible channels are given in the Appendix. The quantity $\langle v_{12}\sigma_{\rm ann}\rangle$ is the sum of all these contributions. Imposing $\langle v_{12}\sigma_{\rm ann}\rangle = 1.9 \times 10^{-9}$ GeV^{-2} dictates the behavior of $\eta_{01}^{(4)}$, which is displayed as a function of the dark matter mass m_0. Of course, as the parameters are numerous, the behavior is bound to be rich and diverse. We cannot describe every bit of it. Also, one has to note from the outset that for a given set of values of the parameters, the solution to the relic-density constraint is not unique: besides positive real solutions (when they exist), we may find negative real or even complex solutions. Indeed, from the physical coefficients in (2.11) and (2.13), one can show that $\langle v_{12}\sigma_{\rm ann}\rangle$ is a sum of quotients of up-to-quartic polynomials in $\eta_{01}^{(4)}$. This means that, ultimately, the relic-density constraint is going to be an algebraic equation in $\eta_{01}^{(4)}$, which has always solutions in the complex plane, but not necessarily on the positive real axis. It is beyond the scope of the present work to investigate systematically the nature and behavior of all the solutions. We are only interested in finding the smallest of the positive real solutions in $\eta_{01}^{(4)}$ when they exist, looking at its behavior and finding out when it is small enough to be perturbative.

Finally, in the decoupling limit m_1 very large and $\theta = 0$ so that there is no annihilation channel of S_0 into S_1 or via S_1 to standard model light fermions, we recover the results of the one-singlet dark matter extension to the standard model[26].

A. Small mixing angle and very weak dark matter—Higgs coupling

Let us describe briefly, and only partly as mentioned, how the mutual S_0—S_1 coupling constant $\eta_{01}^{(4)}$ behaves as a function of the S_0 mass m_0. We start by a small mixing angle, say $\theta = 10°$, and a very weak mutual S_0—Higgs coupling constant, say $\lambda_0^{(4)} = 0.01$. Let us also fix the S_1 mass first at the small value $m_1 = 10$ GeV. The corresponding behavior of $\eta_{01}^{(4)}$ vs m_0 is shown in Fig. 1. The range of m_0 shown is from 0.1 GeV to 200 GeV, cut in four intervals to allow for "local" features to be displayed.[1] We see that the relic-density constraint on S_0 annihilation has

[1]A logplot in this descriptive study is not advisable.

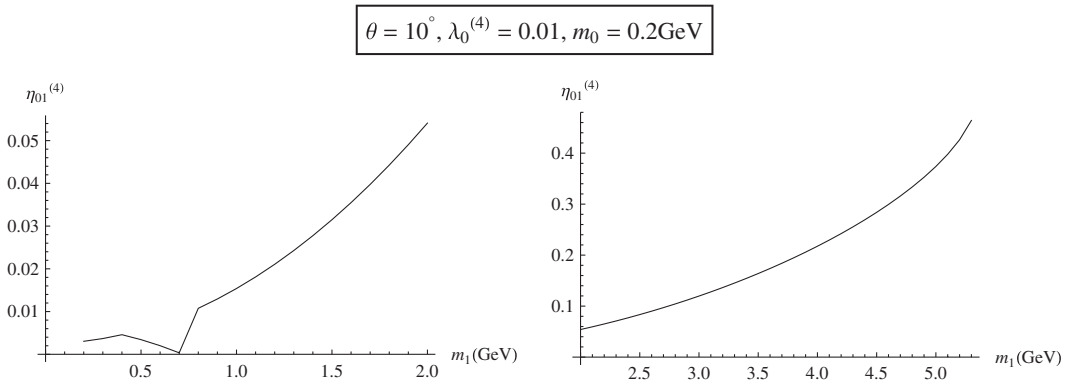

FIG. 2. $\eta_{01}^{(4)}$ vs m_1 for very light S_1, small mixing and very small WIMP-Higgs coupling.

no positive real solution for $m_0 \lesssim 1.3$ GeV, and so, with these very small masses, S_0 cannot be a dark matter candidate. In other words, for $m_1 = 10$ GeV, the particle S_0 cannot annihilate into the lightest fermions only in a way compatible with the relic-density constraint; inclusion of the c-quark is necessary. Note that right about $m_0 \simeq 1.3$ GeV, the c threshold, the mutual coupling constant $\eta_{01}^{(4)}$ starts at about 0.8, a value, while perturbative, that is roughly 80-fold larger than the mutual S_0—Higgs coupling constant $\lambda_0^{(4)}$. Then $\eta_{01}^{(4)}$ decreases, steeply first, more slowly as we cross the τ mass towards the b mass. Just before $m_1/2$, the coupling $\eta_{01}^{(4)}$ hops onto another solution branch that is just emerging from negative territory, gets back to the first one at precisely $m_1/2$ as this latter carries now smaller values, and then jumps up again onto the second branch as the first crosses the m_0-axis down. It goes up this branch with a moderate slope until m_0 becomes equal to m_1, a value at which the S_1 annihilation channel opens. Right beyond m_1, there is a sudden fall to a value $\eta_{01}^{(4)} \simeq 0.0046$ that is about half the value of $\lambda_0^{(4)}$, and $\eta_{01}^{(4)}$ stays flat till $m_0 \simeq 45$ GeV where it starts increasing, sharply after 60 GeV. In the mass interval $m_0 \simeq 66$ GeV–79 GeV, there is a ''desert'' with no positive real solutions to the relic-density constraint, hence no viable dark matter candidate. Beyond $m_0 \simeq 79$ GeV, the mutual coupling constant $\eta_{01}^{(4)}$ keeps increasing monotonously, with a small notch at the W mass and a less noticeable one at the Z mass.

Note that for this value of m_1 (10 GeV), all values reached by $\eta_{01}^{(4)}$ in the mass range considered, however large or small with respect to $\lambda_0^{(4)}$, are perturbatively acceptable. This may not be the case for larger values of m_1. For example, for $m_1 = 30$ GeV while keeping $\theta = 10°$ and $\lambda_0^{(4)} = 0.01$, the mutual coupling constant $\eta_{01}^{(4)}$ starts at $m_0 \simeq 1.5$ GeV with the very large value 89.8 and decreases very sharply right after, to 2.04 at about 1.6 GeV. The rest of the overall features are similar to the case $m_1 = 10$ GeV.

Because of the very-small-m_0 deserts described and visible on Fig. 1, one may ask whether the model ever allows for very light dark matter. To look into this, we fix m_0 at small values and let m_1 vary. Take, for example, $m_0 = 0.2$ GeV and see Fig. 2. The allowed S_0 annihilation channels are the very light fermions e, u, d, μ, and s, plus S_1 when $m_1 < m_0$. Note that we still have $\theta = 10°$ and $\lambda_0^{(4)} = 0.01$. Qualitatively, we notice that in fact, there are no solutions for $m_1 < m_0$, a mass at which $\eta_{01}^{(4)}$ takes the very small value $\simeq 0.003$. It goes up a solution branch and leaves it at $m_1 \simeq 0.4$ GeV to descend on a second branch that enters negative territory at $m_1 \simeq 0.7$ GeV, forcing $\eta_{01}^{(4)}$ to return onto the first branch. There is an accelerated increase until $m_1 \simeq 5$ GeV, a value at which $\eta_{01}^{(4)} \simeq 0.5$. And then a desert, no positive real solutions, no viable dark matter.

Increasing m_0 until about 1.3 GeV does not change these overall features: some ''movement'' for very small values of m_1 and then an accelerated increase until reaching a desert with a lower bound that changes with m_0. For example, the desert starts at $m_1 \simeq 6.8$ GeV for $m_0 = 0.6$ GeV and $m_1 \simeq 7.3$ GeV for $m_0 = 1.2$ GeV. Note that in all these cases where $m_0 \lesssim 1.3$ GeV, all values of $\eta_{01}^{(4)}$ are perturbative. Therefore, the model can very well accommodate very light dark matter with a restricted range of S_1 masses.

However, the situation changes after the inclusion of the τ annihilation channel. Indeed, as Fig. 3 shows, for $m_0 = 1.4$ GeV, though the overall shape of the behavior of $\eta_{01}^{(4)}$ as a function of m_1 is qualitatively the same, the desert threshold is pushed significantly higher, to $m_1 \simeq 20$ GeV. But more significantly, $\eta_{01}^{(4)}$ starts to be larger than one already at $m_1 \simeq 17$ GeV, therefore loosing perturbativity. For $m_0 = 1.5$ GeV, the desert is effectively erased as we have a sudden jump to highly nonperturbative values of $\eta_{01}^{(4)}$ right after $m_1 \simeq 28$ GeV. Such a behavior stays with larger values of m_0. But for $m_1 \lesssim 20$ GeV (case $m_0 = 1.5$ GeV), the values of $\eta_{01}^{(4)}$ are smaller than 1 and physical use of the model is possible if needed.

In passing, one may wander how is it that for $m_0 = 1.5$ GeV in Fig. 3, $\eta_{01}^{(4)}$ stays flat at about 90 for

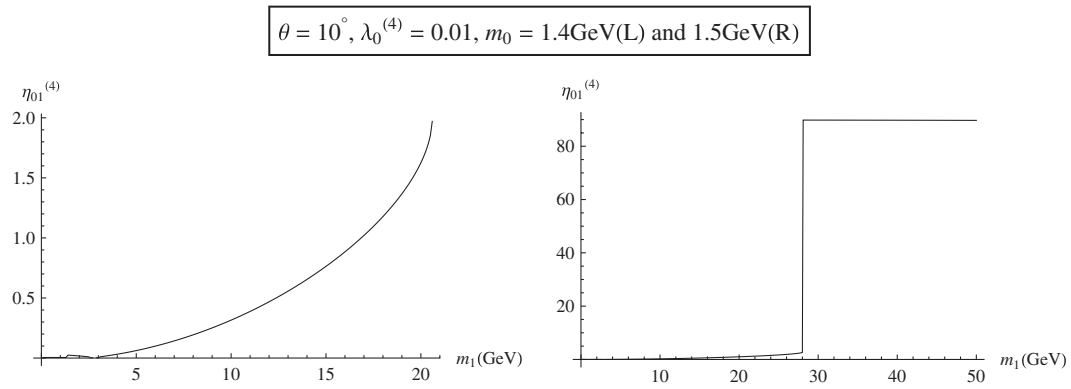

FIG. 3. $\eta_{01}^{(4)}$ vs m_1 for m_0 above τ threshold.

$m_1 \gtrsim 28$ GeV. Remember that the annihilation of S_0 into fermions proceeds via two s-channel diagrams mediated by h and S_1. For θ small, the annihilation cross section via S_1 exchange is smaller than 10^{-2} pb. In fact, it is approximately given by

$$\sigma_{\rm ann}(\text{via}\, S_1) \sim \left(\frac{30\,\text{GeV}}{m_1}\right)^4 \times \frac{(\eta_{01}^{(4)})^2}{[1+10^{-2}(\eta_{01}^{(4)})^4(30\,\text{GeV}/m_1)^4]} \times 10^{-2}\,\text{pb}. \tag{3.3}$$

For $m_h = 138$ GeV, the Higgs-mediated annihilation process is approximately given by

$$\sigma_{\rm ann}(\text{via}\, h) \sim \frac{(\eta_{01}^{(4)})^2}{[1+2\times 10^{-8}(\eta_{01}^{(4)})^4]} \times 10^{-4}\ \text{pb}. \tag{3.4}$$

Note that in deriving these approximate expressions, we used Eqs. (2.11) and (2.13). Also, the channels mediated by the mixing between h and S_1 are suppressed by a factor of order m_1^2/m_h^2 compared to $\sigma_{\rm ann}(\text{via}\, S_1)$. Thus, we see that the only possible way to get the observed dark matter relic density is via the Higgs-dominated channel for $\eta_{01}^{(4)} \sim 90$, regardless of the value of m_1.

B. Small mixing angle and larger dark matter—Higgs couplings

What are the effects of the relic-density constraint when we vary the parameter $\lambda_0^{(4)}$? Let us keep the Higgs—S_1 mixing angle small ($\theta = 10°$) and increase $\lambda_0^{(4)}$, first to 0.2 and later to 1. For $\lambda_0^{(4)} = 0.2$, Fig. 4 shows the behavior of $\eta_{01}^{(4)}$ as a function of the dark matter mass m_0 when $m_1 = 20$ GeV. We see that $\eta_{01}^{(4)}$ starts at $m_0 \simeq 1.4$ GeV with a value of about 1.95. It decreases with a sharp change of slope at the b threshold, then makes a sudden dive at about 5 GeV, a change of branch at $m_1/2$ down till about 12 GeV where it jumps up back onto the previous branch just before going to cross into negative territory. It drops sharply at $m_0 = m_1$ and then increases slowly until $m_0 \simeq 43.3$ GeV. Beyond, there is nothing, a desert. This is of course different from the situation of very small $\lambda_0^{(4)}$ like in Fig. 1 above: here we see some kind of natural dark-matter mass "confinement" to small-moderate viable[2] values.

For larger values of m_1 with $\lambda_0^{(4)} = 0.2$, one obtains roughly the same behavior. However, not all values of $\eta_{01}^{(4)}$ are perturbative. For example, for $m_1 = 60$ GeV, the mutual coupling $\eta_{01}^{(4)}$ starts very high ($\simeq 85$) at $m_0 \simeq 1.5$ GeV, and then decreases rapidly. There is a usual change of branches and a desert starting at about 49 GeV. What is peculiar here is that, in contrast with previous situations, the desert starts at a mass $m_0 < m_1$, i.e., before the opening of the S_1 annihilation channel. In other words, the dark-matter is annihilating into the light fermions only and the model is perturbatively viable in the range 20 GeV–49 GeV.

The case $\lambda_0^{(4)} = 1$ with $m_1 = 20$ GeV is displayed in Fig. 5. There are no solutions below $m_0 \simeq 1.5$ GeV at which $\eta_{01}^{(4)} \simeq 1.8$. From this value, $\eta_{01}^{(4)}$ slips down very quickly to pick up less abruptly when crossing the τ threshold. There is a significant change in the slope at the crossing of the b mass. Note the absence of a solution at $m_1/2$, which is a new feature, present for other values of m_1 not displayed here. This is due to the fact that the $h - S_1$ interference term in the annihilation process into a $b\bar{b}$ pair, which dominates here, is not present to balance the pure h and S_1 contributions. Therefore, $\eta_{01}^{(4)}$ has to go complex to satisfy the relic-density constraint. However, slightly away from $m_1/2$, this interference term, sensitive to small changes, comes in force and is capable of bringing about a positive real solution. Beyond $m_1/2$, there is a slight change in the downward slope, a change of solution branch, and that goes until 14.5 GeV where $\eta_{01}^{(4)}$ jumps to

[2]Note that the values of $\eta_{01}^{(4)}$ for 1.6 GeV $\lesssim m_0 \lesssim$ 43.3 GeV are all perturbative.

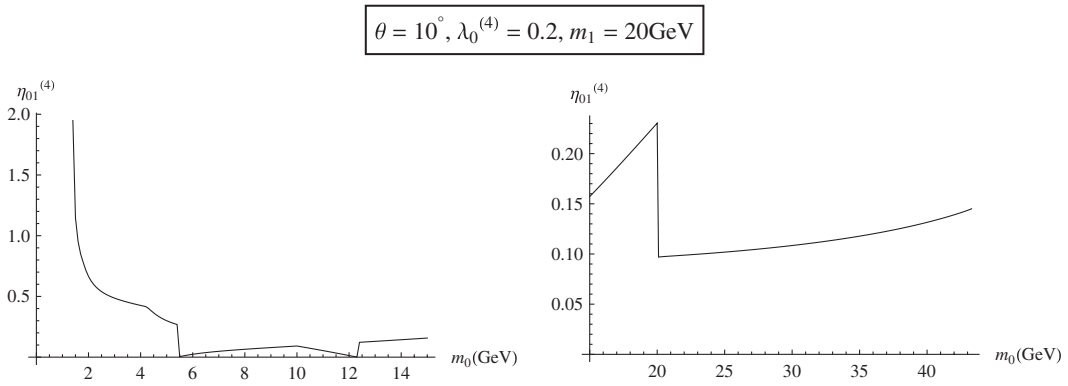

FIG. 4. $\eta_{01}^{(4)}$ vs m_0 for small mixing, moderate m_1 and WIMP-Higgs coupling.

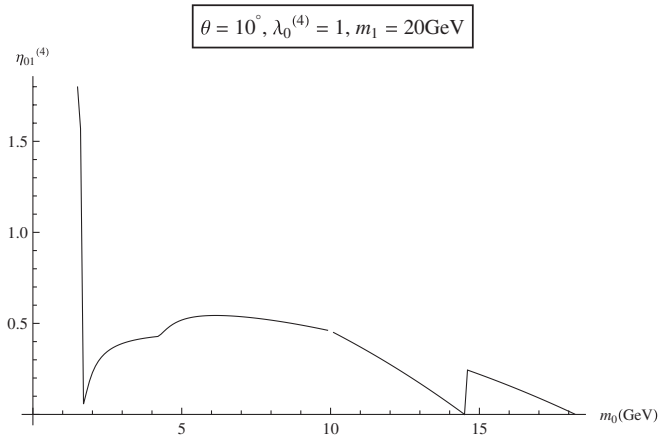

FIG. 5. $\eta_{01}^{(4)}$ vs m_0 for medium m_1, small mixing and large WIMP-higgs coupling.

catch up with the previous branch. It goes down this branch until about 18 GeV, where the desert starts.

We have studied the behavior of $\eta_{01}^{(4)}$ as a function of m_0 for other values of m_1 between 20 GeV and 100 GeV while keeping $\theta = 10°$ and $\lambda_0^{(4)} = 1$. For $m_1 \lesssim 79.2$ GeV, the behavior is qualitatively quite similar to that shown in Fig. 5, but beyond this mass, $\eta_{01}^{(4)}$ jumps onto a highly nonperturbative branch that starts at small and moderate values of m_0. This highly nonperturbative region stretches in size as m_1 increases. For example, for $m_1 = 79.3$ GeV, this region is roughly between 13 GeV and 16 GeV. Otherwise, outside this region, the behavior of $\eta_{01}^{(4)}$ is similar to the one displayed in Fig. 5.

C. Larger mixing angles

Last in this descriptive study is to see the effects of larger values of the S_1—Higgs mixing angle θ. We give it here the value $\theta = 40°$ and tune back the mutual S_0—Higgs coupling constant $\lambda_0^{(4)}$ to the very small value 0.01. Figure 6 shows the behavior of $\eta_{01}^{(4)}$ as a function of m_0 for $m_1 = 20$ GeV. One recognizes features similar to those of the case $\theta = 10°$, though coming in different relative sizes. The very-small-m_0 desert ends at about 0.3 GeV. There are by-now familiar features at the c and b masses, $m_1/2$ and m_1. Two relatively small forbidden intervals (deserts) appear for relatively large values of the dark matter mass: 67.3 GeV–70.9 GeV and 79.4 GeV–90.8 GeV. The W mass is in the forbidden region, but there is action as we cross the Z mass. Other values of m_1, not displayed because of space, behave similarly with an additional effect, namely a sudden drop in slope at $m_0 = (m_h + m_1)/2$ coming from the ignition of S_0 annihilation into S_1 and Higgs.

We have also worked out the cases $\lambda_0^{(4)} = 0.2$ and 1 for $\theta = 40°$. The case $\lambda_0^{(4)} = 0.2$ is displayed in Fig. 7 and presents differences with the corresponding small-mixing situation $\theta = 10°$. Indeed, for $m_1 = 20$ GeV, the first feature we notice is a smoother behavior; compare with Fig. 4. Here, $\eta_{01}^{(4)}$ starts at $m_0 \simeq 0.3$ GeV with the small value $\simeq 0.016$ and goes up, faster at the c mass and with a small effect at the b mass. It increases very slowly until $m_1/2$ and decreases very slowly until $m_0 = m_1$, and then there is a sudden change of branch followed immediately by a desert.[3] So here, too, the model naturally confines the mass of a viable dark matter to small-moderate values, a dark matter particle annihilating into light fermions only. What is also noticeable is that there is stability of $\eta_{01}^{(4)}$ around the value of $\lambda_0^{(4)}$ in the interval 1.5 GeV–20 GeV ($= m_1$ here).

The case $m_1 = 60$ GeV presents also overall similarities as well as noticeable differences with the corresponding case $\theta = 10°$. The first difference is that all values of $\eta_{01}^{(4)}$ are perturbative. This latter starts at $m_0 \simeq 1.4$ GeV with the value ~ 0.75, goes down and jumps to catch up with another solution branch emerging from negative territory when crossing the τ mass. It increases, kicking up when crossing the b-quark mass. It changes slope down at $m_1/2$

[3]Except for the very tiny interval 78.5 GeV–79.0 GeV not displayed on Fig. 7.

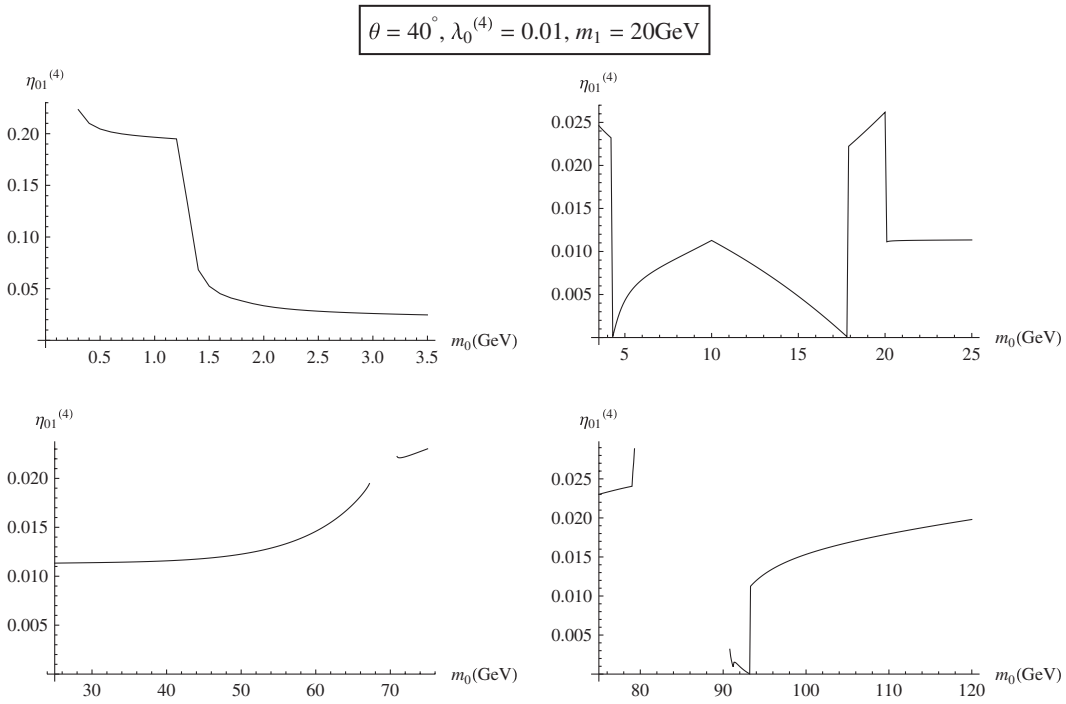

FIG. 6. $\eta_{01}^{(4)}$ vs m_0 for moderate m_1, moderate mixing and small WIMP-Higgs coupling.

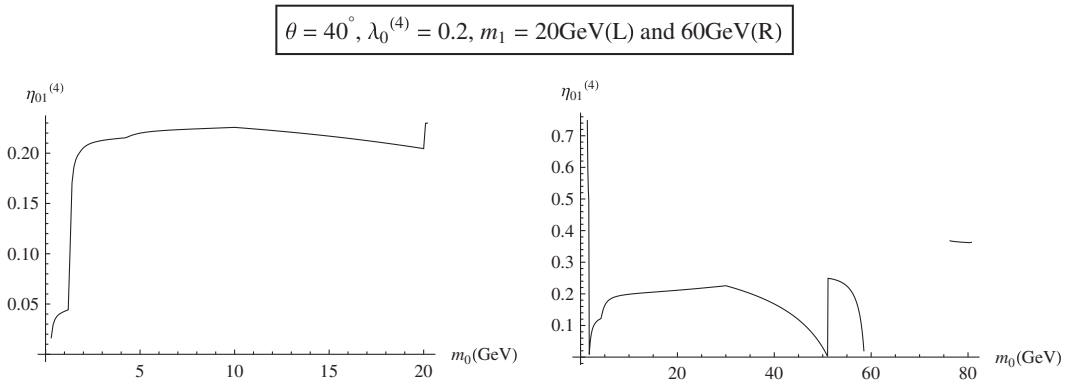

FIG. 7. $\eta_{01}^{(4)}$ vs m_0 for moderate (L) and larger (R) m_1, large mixing and moderate WIMP-Higgs coupling.

and goes to zero at about 51 GeV. It jumps up onto another branch that goes down to zero also at about 58.6 GeV, just below m_1, and then there is a desert, except for the small interval 76.3 GeV–80.5 GeV.

The case $\lambda_0^{(4)} = 1$ shows global similarities with the previous case. All values of $\eta_{01}^{(4)}$ are perturbative and the mass range is naturally confined to the interval 0.2 GeV–20 GeV for $m_1 = 20$ GeV, and 1.4 GeV–52.3 GeV for $m_1 = 60$ GeV. There is action at the usual masses and, in particular, there are no solutions at $m_0 = m_1/2$, like in the case $\theta = 10°$. We note here, too, the quasiconstancy of $\eta_{01}^{(4)}$ for most of the available range.

Finally, we mention that we have also worked out larger mixing angles, notably $\theta = 75°$. In general, these cases do not display any new features worth discussing: the overall behavior is mostly similar to what we have seen, with expected relative variations in size.

IV. DARK MATTER DIRECT DETECTION

Experiments like CDMS II [28], XENON 10/100 [8,27], DAMA/LIBRA [2] and CoGeNT [3] search directly for a dark matter signal. Such a signal would typically come from the elastic scattering of a dark matter WIMP off a nonrelativistic nucleon target. However, throughout the years such experiments have not yet detected an unambiguous signal, but rather yielded increasingly stringent exclusion bounds on the dark matter–nucleon elastic-scattering total cross section $\sigma_{\rm det}$ in terms of the dark matter mass m_0.

In order for a theoretical dark matter model to be viable, it has to satisfy these bounds. It is therefore natural to inquire whether the model we present in this work has any capacity of describing dark matter. Hence, we have to calculate $\sigma_{\rm det}$ as a function of m_0 for different values of the parameters $(\theta, \lambda_0^{(4)}, m_1)$ and project its behavior against the experimental bounds. We will limit ourselves to the region 0.1 GeV–100 GeV as we are interested in light dark matter. As experimental bounds, we will use the results from CDMSII and XENON100, as well as the future projections of SuperCDMS [30] and XENON1T [31]. The results of CoGeNT, DAMA/LIBRA, and CRESST will be discussed elsewhere [32]. As the figures below show [38], in the region of our interest, XENON100 is only slightly tighter than CDMSII, SuperCDMS significantly lower, and XENON1T the most stringent by far. But it is important to note that all these results lose reasonable predictability in the very light sector, say below 5 GeV.

The scattering of S_0 off a SM fermion f occurs via the t-channel exchange of the SM Higgs and S_1. In the nonrelativistic limit, the effective Lagrangian describing this interaction reads

$$\mathcal{L}^{\rm (eff)}_{S_0-f} = a_f \bar{f} f S_0^2, \tag{4.1}$$

where

$$a_f = -\frac{m_f}{2v}\left[\frac{\lambda_0^{(3)}\cos\theta}{m_h^2} - \frac{\eta_{01}^{(3)}\sin\theta}{m_1^2}\right]. \tag{4.2}$$

In this case, the total cross-section for this process is given by

$$\sigma_{S_0 f\to S_0 f} = \frac{m_f^4}{4\pi(m_f+m_0)^2 v^2}\left[\frac{\lambda_0^{(3)}\cos\theta}{m_h^2} - \frac{\eta_{01}^{(3)}\sin\theta}{m_1^2}\right]^2. \tag{4.3}$$

At the nucleon level, the effective interaction between a nucleon $N = p$ or n and S_0 has the form

$$\mathcal{L}^{\rm (eff)}_{S_0-N} = a_N \bar{N} N S_0^2, \tag{4.4}$$

where the effective nucleon—S_0 coupling constant is given by

$$a_N = \frac{(m_N - \frac{7}{9}m_B)}{v}\left[\frac{\lambda_0^{(3)}\cos\theta}{m_h^2} - \frac{\eta_{01}^{(3)}\sin\theta}{m_1^2}\right]. \tag{4.5}$$

In this relation, m_N is the nucleon mass and m_B the baryon mass in the chiral limit [26]. The total cross section for nonrelativistic S_0—N elastic scattering is therefore

$$\sigma_{\rm det} \equiv \sigma_{S_0 N\to S_0 N} = \frac{m_N^2(m_N - \frac{7}{9}m_B)^2}{4\pi(m_N+m_0)^2 v^2}\left[\frac{\lambda_0^{(3)}\cos\theta}{m_h^2} - \frac{\eta_{01}^{(3)}\sin\theta}{m_1^2}\right]^2. \tag{4.6}$$

The rest of this section is devoted to a brief discussion of the behavior of $\sigma_{\rm det}$ as a function of m_0. We will of course impose the relic-density constraint on the dark matter annihilation cross section (3.2). But in addition, we will require that the coupling constants are perturbative, and so impose the additional requirement $0 \le \eta_{01}^{(4)} \le 1$. Here, too, the choices of the sets of values of the parameters $(\theta, \lambda_0^{(4)}, m_1)$ can by no means be exhaustive but only indicative. Furthermore, though a detailed description of the behavior of $\sigma_{\rm det}$ could be interesting in its own right, we will refrain from doing so in this work as there is no need for it, and content ourselves with mentioning overall features and trends. Generally, as m_0 increases, the detection cross section $\sigma_{\rm det}$ starts from high values, slopes down to minima that depend on the parameters and then picks up moderately. There are features and action at the usual mass thresholds, with varying sizes and shapes. Excluded regions are there, those coming from the relic-density constraint and new ones originating from the additional perturbativity requirement. Close to the upper boundary of the mass interval considered in this study, there is no universal behavior to mention as in some cases $\sigma_{\rm det}$ will increase monotonously and, in some others, it will decrease or "not be there" at all. Let us finally remark that the logplots below may not show these general features clearly, as these latter are generally distorted.

Let us start with the small Higgs—S_1 mixing angle $\theta = 10°$ and the very weak mutual S_0—Higgs coupling $\lambda_0^{(4)} = 0.01$. Figure 8 shows the behavior of $\sigma_{\rm det}$ vs m_0 in the case $m_1 = 20$ GeV. We see that for the two mass intervals 20 GeV–65 GeV and 75 GeV–100 GeV, plus an almost singled-out dip at $m_0 = m_1/2$, the elastic scattering cross section is below the projected sensitivity of SuperCDMS. However, XENON1T will probe all these masses, except $m_0 \simeq 58$ GeV and 85 GeV.

Also, as we see in Fig. 8, most of the mass range for very light dark matter is excluded for these values of the parameters. Is this systematic? In general, smaller values of m_1 drive the predictability ranges to the lighter sector of

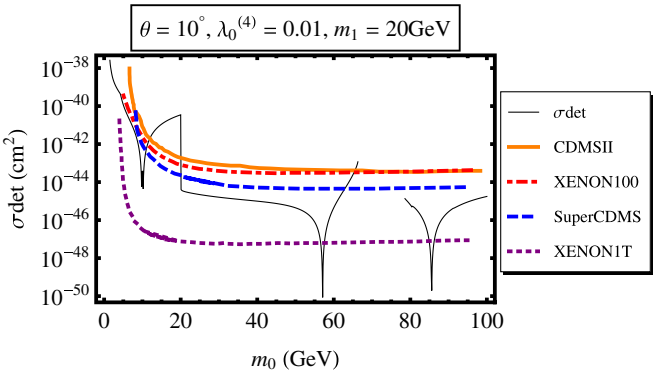

FIG. 8 (color online). Elastic $N - S_0$ scattering cross section as a function of m_0 for moderate m_1, small mixing and small WIMP-Higgs coupling.

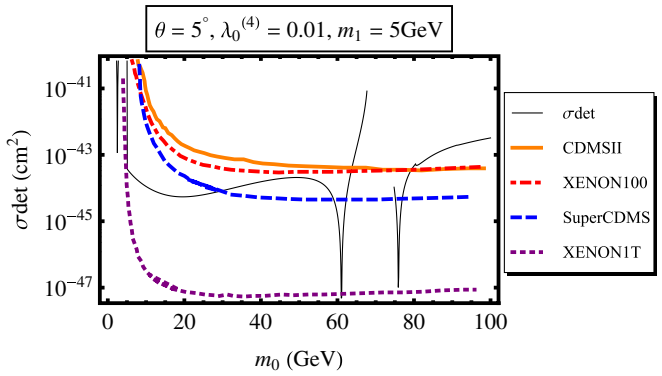

FIG. 9 (color online). Elastic $N - S_0$ scattering cross section as a function of m_0 for light S_1, small mixing and small WIMP-Higgs coupling.

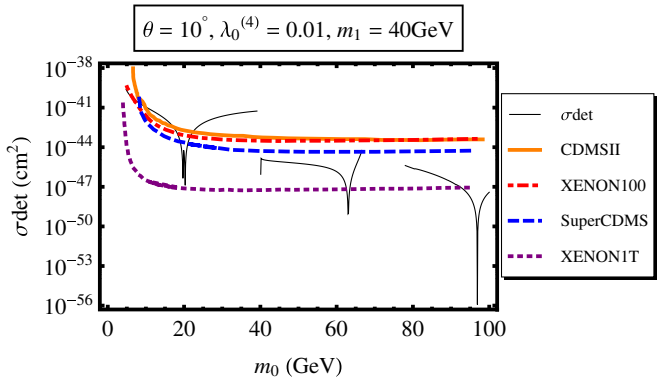

FIG. 10 (color online). Elastic $N - S_0$ scattering cross section as a function of m_0 for moderate m_1, small mixing and small WIMP-Higgs coupling.

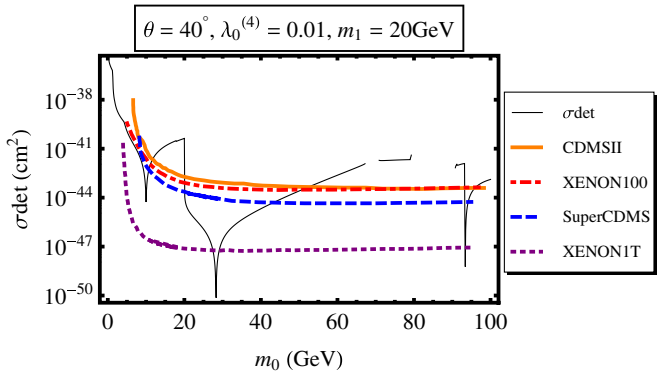

FIG. 11 (color online). Elastic $N - S_0$ scattering cross section as a function of m_0 for moderate m_1, large mixing and small WIMP-Higgs coupling.

the dark matter masses. Figure 9 illustrates this pattern. We have taken $m_1 = 5$ GeV just above the lighter-quarks threshold. In the small-mass region, we see that SuperCDMS is passed in the range 5 GeV–30 GeV. Again, all this mass ranges will be probed by XENON1T experiment, except a sharp dip at $m_0 = m_1/2 = 2.5$ GeV,

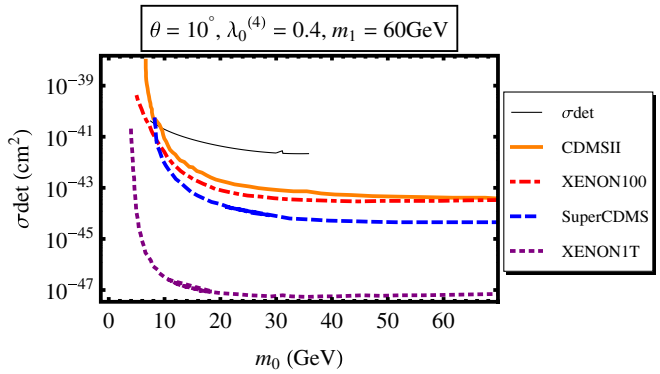

FIG. 12 (color online). Elastic cross section $\sigma_{\rm det}$ vs m_0 for heavy S_1, small mixing and relatively large WIMP-Higgs coupling.

but for such a very light mass, the experimental results are not without ambiguity.

Reversely, increasing m_1 shuts down possibilities for very light dark matter and thins the intervals as it drives the predicted masses to larger values. For instance, in Fig. 10 where $m_1 = 40$ GeV, in addition to the dip at $m_1/2$ that crosses SuperCDMS but not XENON1T, we see acceptable masses in the ranges 40 GeV–65 GeV and 78 GeV—up. Here, too, the intervals narrow as we descend, surviving XENON1T as spiked dips at 62 GeV and around 95 GeV.

A larger mutual coupling constant $\lambda_0^{(4)}$ has the general effect of squeezing the acceptable intervals of m_0 by pushing the values of $\sigma_{\rm det}$ up. Also, increasing the mixing angle θ has the general effect of increasing the value of $\sigma_{\rm det}$. Figure 11 shows this trend for $\theta = 40°$; compare with Fig. 8. The only allowed masses by the current bounds of CDMSII and XENON100 are between 20 GeV and 50 GeV, the narrow interval around $m_1/2$, and another very sharp one, at about 94 GeV. The projected sensitivity of XENON1T will probe all mass ranges except those at $m_0 \simeq 30$ GeV and 94 GeV.

Finally, it happens that there are regions of the parameters for which the model has no predictability. See Fig. 12 for illustration. We have combined the effects of increasing the values of the two parameters $\lambda_0^{(4)}$ and m_1. As we see, we barely get something at $m_1/2$, and that cannot even cross XENON100 down to SuperCDMS.

V. CONCLUDING REMARKS

In this work, we presented a plausible scenario for light cold dark matter, i.e., for masses in the range 0.1 GeV–100 GeV. This latter consists in enlarging the standard model with two gauge-singlet $\mathbb{Z}_2$-symmetric scalar fields. One is the dark matter field S_0, stable, while the other undergoes spontaneous symmetry breaking, resulting in the physical field S_1. This opens additional channels through which S_0 can annihilate, hence reducing

its number density. The model is parametrized by three quantities: the physical mutual coupling constant $\lambda_0^{(4)}$ between S_0 and the Higgs, the mixing angle θ between S_1 and the Higgs and the mass m_1 of the particle S_1. We first imposed on S_0 annihilation cross section the constraint from the observed dark matter relic density and studied its effects through the behavior of the physical mutual coupling constant $\eta_{01}^{(4)}$ between S_0 and S_1 as a function of the dark matter mass m_0. Apart from forbidden regions (deserts) and others where perturbativity is lost, we find that for most values of the three parameters, there are viable solutions in the small-moderate mass ranges of the dark matter sector. Deserts are found for most of the ranges of the parameters whereas perturbativity is lost mainly for larger values of m_1. Through the behavior of $\eta_{01}^{(4)}$, we could see the mass thresholds which mostly affect the annihilation of dark matter, and these are at the c, τ, and b masses, as well as $m_1/2$ and m_1.

The current experimental bounds from CDMSII and XENON100 put a strong constraint on the S_0 masses in the range between 10 to 20 GeV. For small values of m_1, very light dark matter is viable, with a mass as small as 1 GeV. This is of course useful for understanding the results of the experiments DAMA/LIBRA, CoGeNT, CRESST as well as the recent data of the Fermi Gamma Ray Space Telescope. The projected sensitivity of future WIMP direct searches such as XENON1T will probe all the S_0 masses between 5 GeV and 100 GeV.

Also, in our analysis of direct detection, we have constrained the dark matter mass regions to be consistent with perturbativity ($\eta_{01}^{(4)} \leq 1$). This makes the higher-order corrections less than $1/4\pi^2 \sim 2.5\%$. A one-sigma uncertainty in the relic density, which is larger than the loop corrections even for coupling constants equal to one, will not change significantly our results. Furthermore, the QCD radiative corrections to the quark final states are of order $\alpha_s/\pi \sim 4\%$. However, the corresponding annihilation cross section is smaller by at least a factor of 10 compared to the annihilation into S_1, which results in a less-than-0.4% correction to the relic density. If future WMAP measurements of WIMP relic density reach the precision level of 1%, then one would need to consider the effect of loop corrections for couplings in the scalar sector of order one.

The next step to take is to test the model against the phenomenological constraints. Indeed, one important feature of the model is that it mixes the S_1 field with the Higgs. This must have implications on the Higgs detection through the measurable channels. Current experimental bounds from LEP II data can be used to constrain our mixing angle θ, and possibly other parameters. In addition, a very light S_0 and/or S_1 will contribute to the invisible decay of J/ψ and Υ mesons and can lead to a significant branching fraction. In our model, these two mesons will not have an invisible channel if taken in the $1s$ state; one has to see into the $3s$ state. Other light mesons can be considered, like the B_s and B^+ mesons. These constraints can be injected back into the model and restrain further its domain of validity. Such issues are under current investigation [32].

Also, in this work, the S_1 vacuum expectation value v_1 was taken equal to 100 GeV, but *a priori*, nothing prevents us from considering other scales. However, taking v_1 much larger than the electroweak scale requires $\eta_{01}^{(4)}$ to be very small, which will result in the suppression of the crucial annihilation channel $S_0S_0 \rightarrow S_1S_1$. Also, we have fixed the Higgs mass to $m_h = 138$ GeV, which is consistent with the current acceptable experimental bounds [33]. Yet, it can be useful to ask here too what the effect of changing this mass would be.

Finally, in this study, besides the dark matter field S_0, only one extra field has been considered. Naturally, one can generalize the investigation to include N such fields and discuss the cosmology and particle phenomenology in terms of N. It just happens that the model is rich enough to open new possibilities in the quest of dark matter worth pursuing.

APPENDIX: DARK MATTER ANNIHILATION CROSS SECTIONS

The cross sections related to the annihilation of S_0 into the scalar particles are as follows. For the hh channel, we have

$$
\begin{aligned}
v_{12}\sigma_{S_0S_0\rightarrow hh} = \frac{\sqrt{m_0^2 - m_h^2}}{64\pi m_0^3}\Theta(m_0 - m_h)\Bigg[& (\lambda_0^{(4)})^2 + \frac{4\lambda_0^{(4)}(\lambda_0^{(3)})^2}{m_h^2 - 2m_0^2} + \frac{2\lambda_0^{(4)}\lambda_0^{(3)}\lambda^{(3)}}{4m_0^2 - m_h^2} + \frac{2\lambda_0^{(4)}\lambda_1^{(3)}\eta_{01}^{(3)}(4m_0^2 - m_1^2)}{(4m_0^2 - m_1^2)^2 + \epsilon_1^2} + \frac{4(\lambda_0^{(3)})^4}{(m_h^2 - 2m_0^2)^2} \\
& + \frac{4\lambda^{(3)}(\lambda_0^{(3)})^3}{(4m_0^2 - m_h^2)(m_h^2 - 2m_0^2)} + \frac{4(\lambda_0^{(3)})^2\lambda_1^{(3)}\eta_{01}^{(3)}(4m_0^2 - m_1^2)}{[(4m_0^2 - m_1^2)^2 + \epsilon_1^2](m_h^2 - 2m_0^2)} + \frac{(\lambda^{(3)})^2(\lambda_0^{(3)})^2}{(4m_0^2 - m_h^2)^2} + \frac{(\lambda_1^{(3)})^2(\eta_{01}^{(3)})^2}{(4m_0^2 - m_1^2)^2 + \epsilon_1^2} \\
& + \frac{2\lambda_0^{(3)}\lambda_1^{(3)}\lambda^{(3)}\eta_{01}^{(3)}(4m_0^2 - m_1^2)}{[(4m_0^2 - m_1^2)^2 + \epsilon_1^2](4m_0^2 - m_h^2)}\Bigg].
\end{aligned}
\tag{A1}
$$

The Θ function is the step function. For the S_1S_1 channel, we have the result

$$v_{12}\sigma_{S_0S_0\to S_1S_1} = \frac{\sqrt{m_0^2 - m_1^2}}{64\pi m_0^3}\Theta(m_0 - m_1)\Big[(\eta_{01}^{(4)})^2 + \frac{4\eta_{01}^{(4)}(\eta_{01}^{(3)})^2}{m_1^2 - 2m_0^2} + \frac{2\eta_{01}^{(4)}\eta_{01}^{(3)}\eta_1^{(3)}}{4m_0^2 - m_1^2} + \frac{2\eta_{01}^{(4)}\lambda_0^{(3)}\lambda_2^{(3)}(4m_0^2 - m_h^2)}{(4m_0^2 - m_h^2)^2 + \epsilon_h^2}$$
$$+ \frac{4(\eta_{01}^{(3)})^4}{(m_1^2 - 2m_0^2)^2} + \frac{4(\eta_{01}^{(3)})^3\eta_1^{(3)}}{(4m_0^2 - m_1^2)(m_1^2 - 2m_0^2)} + \frac{4(\eta_{01}^{(3)})^2\lambda_0^{(3)}\lambda_2^{(3)}(4m_0^2 - m_h^2)}{[(4m_0^2 - m_h^2)^2 + \epsilon_h^2](m_1^2 - 2m_0^2)} + \frac{(\eta_{01}^{(3)})^2(\eta_1^{(3)})^2}{(4m_0^2 - m_1^2)^2}$$
$$+ \frac{(\lambda_0^{(3)})^2(\lambda_2^{(3)})^2}{(4m_0^2 - m_h^2)^2 + \epsilon_h^2} + \frac{2\eta_{01}^{(3)}\eta_1^{(3)}\lambda_0^{(3)}\lambda_2^{(3)}(4m_0^2 - m_h^2)}{[(4m_0^2 - m_h^2)^2 + \epsilon_h^2](4m_0^2 - m_1^2)}\Big]. \tag{A2}$$

For the hS_1 channel, we have

$$v_{12}\sigma_{S_0S_0\to S_1h} = \frac{\sqrt{[4m_0^2 - (m_h - m_1)^2][4m_0^2 - (m_h + m_1)^2]}}{128\pi m_0^4}\Theta(2m_0 - m_h - m_1)\Big[(\lambda_{01}^{(4)})^2 + \frac{8\lambda_{01}^{(4)}\eta_{01}^{(3)}\lambda_0^{(3)}}{m_h^2 + m_1^2 - 4m_0^2}$$
$$+ \frac{2\lambda_{01}^{(4)}\lambda_0^{(3)}\lambda_1^{(3)}}{4m_0^2 - m_h^2} + \frac{2\lambda_{01}^{(4)}\eta_{01}^{(3)}\lambda_2^{(3)}}{4m_0^2 - m_1^2} + \frac{16(\eta_{01}^{(3)})^2(\lambda_0^{(3)})^2}{(m_h^2 + m_1^2 - 4m_0^2)^2} + \frac{8(\lambda_0^{(3)})^2\eta_{01}^{(3)}\lambda_1^{(3)}}{(m_h^2 + m_1^2 - 4m_0^2)(4m_0^2 - m_h^2)}$$
$$+ \frac{8(\eta_{01}^{(3)})^2\lambda_0^{(3)}\lambda_2^{(3)}}{(m_h^2 + m_1^2 - 4m_0^2)(4m_0^2 - m_1^2)} + \frac{(\lambda_0^{(3)})^2(\lambda_1^{(3)})^2}{(4m_0^2 - m_h^2)^2} + \frac{2\eta_{01}^{(3)}\lambda_0^{(3)}\lambda_1^{(3)}\lambda_2^{(3)}}{(4m_0^2 - m_h^2)(4m_0^2 - m_1^2)} + \frac{(\lambda_2^{(3)})^2(\eta_{01}^{(3)})^2}{(4m_0^2 - m_1^2)^2}\Big]. \tag{A3}$$

The annihilation cross section into fermions is

$$v_{12}\sigma_{S_0S_0\to f\bar{f}} = \frac{\sqrt{(m_0^2 - m_f^2)^3}}{4\pi m_0^3}\Theta(m_0 - m_f)\Big[\frac{(\lambda_0^{(3)}\lambda_{hf})^2}{(4m_0^2 - m_h^2)^2 + \epsilon_h^2} + \frac{(\eta_{01}^{(3)}\lambda_{1f})^2}{(4m_0^2 - m_1^2)^2 + \epsilon_1^2}$$
$$+ \frac{2\lambda_0^{(3)}\eta_{01}^{(3)}\lambda_{hf}\lambda_{1f}(4m_0^2 - m_h^2)(4m_0^2 - m_1^2)}{[(4m_0^2 - m_h^2)^2 + \epsilon_h^2][(4m_0^2 - m_1^2)^2 + \epsilon_1^2]}\Big]. \tag{A4}$$

The annihilation cross section into W's is given by

$$v_{12}\sigma_{S_0S_0\to WW} = \frac{\sqrt{m_0^2 - m_w^2}}{16\pi m_0^3}\Theta(m_0 - m_w)\Big[1 + \frac{(2m_0^2 - m_w^2)^2}{2m_w^4}\Big]\Big[\frac{(\lambda_0^{(3)}\lambda_{hw}^{(3)})^2}{(4m_0^2 - m_h^2)^2 + \epsilon_h^2} + \frac{(\eta_{01}^{(3)}\lambda_{1w}^{(3)})^2}{(4m_0^2 - m_1^2)^2 + \epsilon_1^2}$$
$$+ \frac{2\lambda_0^{(3)}\eta_{01}^{(3)}\lambda_{hw}^{(3)}\lambda_{1w}^{(3)}(4m_0^2 - m_h^2)(4m_0^2 - m_1^2)}{[(4m_0^2 - m_h^2)^2 + \epsilon_h^2][(4m_0^2 - m_1^2)^2 + \epsilon_1^2]}\Big]. \tag{A5}$$

Last, the annihilation cross section into Z's is

$$v_{12}\sigma_{S_0S_0\to ZZ} = \frac{\sqrt{m_0^2 - m_z^2}}{8\pi m_0^3}\Theta(m_0 - m_z)\Big[1 + \frac{(2m_0^2 - m_z^2)^2}{2m_z^4}\Big]\Big[\frac{(\lambda_0^{(3)}\lambda_{hz}^{(3)})^2}{(4m_0^2 - m_h^2)^2 + \epsilon_h^2} + \frac{(\eta_{01}^{(3)}\lambda_{1z}^{(3)})^2}{(4m_0^2 - m_1^2)^2 + \epsilon_1^2}$$
$$+ \frac{2\lambda_0^{(3)}\eta_{01}^{(3)}\lambda_{hz}^{(3)}\lambda_{1z}^{(3)}(4m_0^2 - m_h^2)(4m_0^2 - m_1^2)}{[(4m_0^2 - m_h^2)^2 + \epsilon_h^2][(4m_0^2 - m_1^2)^2 + \epsilon_1^2]}\Big]. \tag{A6}$$

The quantities $\epsilon_h = m_h\Gamma_h$ and $\epsilon_1 = m_1\Gamma_1$ are regulators at the respective resonances. The decay rates Γ_h and Γ_1 are calculable in perturbation theory. We have for h

$$
\begin{aligned}
\epsilon_{h\to f\bar{f}} &= \frac{(\lambda_{hf})^2}{8\pi} m_h^2 N_c \left(1-\frac{4m_f^2}{m_h^2}\right)^{3/2} \Theta(m_h-2m_f);\\
\epsilon_{h\to WW} &= \frac{(\lambda_{hw}^{(3)})^2}{8\pi}\left(1-\frac{4m_w^2}{m_h^2}\right)^{1/2}\left[1+\frac{(m_h^2-2m_w^2)^2}{8m_w^4}\right]\Theta(m_h-2m_w);\\
\epsilon_{h\to ZZ} &= \frac{(\lambda_{hz}^{(3)})^2}{4\pi}\left(1-\frac{4m_z^2}{m_h^2}\right)^{1/2}\left[1+\frac{(m_h^2-2m_z^2)^2}{8m_z^4}\right]\Theta(m_h-2m_z);\\
\epsilon_{h\to S_0S_0} &= \frac{(\lambda_0^{(3)})^2}{32\pi}\left(1-\frac{4m_0^2}{m_h^2}\right)^{1/2}\Theta(m_h-2m_0);\\
\epsilon_{h\to S_1S_1} &= \frac{(\lambda_2^{(3)})^2}{32\pi}\left(1-\frac{4m_1^2}{m_h^2}\right)^{1/2}\Theta(m_h-2m_1)
\end{aligned}
\tag{A7}
$$

Here, N_c is equal to 1 for leptons and 3 for quarks. For S_1, we have similar expressions:

$$
\begin{aligned}
\epsilon_{S_1\to f\bar{f}} &= \frac{(\lambda_{1f})^2}{8\pi} m_1^2 N_c \left(1-\frac{4m_f^2}{m_1^2}\right)^{3/2} \Theta(m_1-2m_f);\\
\epsilon_{S_1\to WW} &= \frac{(\lambda_{1w}^{(3)})^2}{8\pi}\left(1-\frac{4m_w^2}{m_1^2}\right)^{1/2}\left[1+\frac{(m_1^2-2m_w^2)^2}{8m_w^4}\right]\Theta(m_1-2m_w);\\
\epsilon_{S_1\to ZZ} &= \frac{(\lambda_{1z}^{(3)})^2}{4\pi}\left(1-\frac{4m_z^2}{m_1^2}\right)^{1/2}\left[1+\frac{(m_1^2-2m_z^2)^2}{8m_z^4}\right]\Theta(m_1-2m_z);\\
\epsilon_{S_1\to S_0S_0} &= \frac{(\eta_{01}^{(3)})^2}{32\pi}\left(1-\frac{4m_0^2}{m_1^2}\right)^{1/2}\Theta(m_1-2m_0);\\
\epsilon_{S_1\to hh} &= \frac{(\lambda_1^{(3)})^2}{32\pi}\left(1-\frac{4m_h^2}{m_1^2}\right)^{1/2}\Theta(m_1-2m_h).
\end{aligned}
\tag{A8}
$$

[1] D. N. Spergel *et al.* (WMAP Collaboration), Astrophys. J. Suppl. Ser. **170**, 377 (2007); A. C. Pope *et al.* (The SDSS Collaboration), Astrophys. J. **607**, 655 (2004).

[2] R. Bernabei, P. Belli, and F. Cappella *et al.* (DAMA/LIBRA Collaboration), arXiv:1007.0595; Eur. Phys. J. C **67**, 39 (2010).

[3] C. E. Aalseth *et al.* (CoGeNT Collaboration), Phys. Rev. Lett. **106**, 131301 (2011).

[4] D. Hooper and L. Goodenough, Phys. Lett. B **697**, 412 (2011).

[5] S. Andreas, T. Hambye, and M. H. G. Tytgat, J. Cosmol. Astropart. Phys. 10 (2008) 034; S. Chang, J. Liu, A. Pierce, N. Weiner, and I. Yavin, J. Cosmol. Astropart. Phys. 08 (2010) 018; R. Essig, J. Kaplan, P. Schuster, and N. Toro, arXiv:1004.0691; S. Andreas, C. Arina, T. Hambye, Fu-Sin Ling, and M. H. G. Tytgat, Phys. Rev. D **82**, 043522 (2010); D. Hooper, J. I. Collar, J. Hall, D. McKinsey, and C. Kelso, Phys. Rev. D **82**, 123509 (2010); R. Foot, Phys. Lett. B **692**, 65 (2010); A. L. Fitzpatrick, D. Hooper, and K. M. Zurek, Phys. Rev. D **81**, 115005 (2010).

[6] R Davé, D. N. Spergel, P. J. Steinhardt, and B. D. Wandelt, Astrophys. J. **547**, 574 (2001).

[7] J. McDonald, Phys. Rev. Lett. **88**, 091304 (2002).

[8] E. Aprile *et al.* (XENON100 Collaboration), Phys. Rev. Lett. **105**, 131302 (2010); arXiv:1005.2615.

[9] J. I. Collar and D. N. McKinsey, arXiv:1005.0838.

[10] D. S. Akerib *et al.* (CDMS Collaboration), Phys. Rev. D **82**, 122004 (2010); Z. Ahmed *et al.* (CDMS Collaboration), Phys. Rev. Lett. **106**, 131302 (2011).

[11] E. M. Drobyshevski, Mod. Phys. Lett. A **23**, 3077 (2008) arXiv:0706.3095; R. Bernabei *et al.*, Eur. Phys. J. C **53**, 205 (2008); N. Bozorgnia, G. B. Gelmini, and P. Gondolo, J. Cosmol. Astropart. Phys. 11 (2010) 019; N. Bozorgnia, G. B. Gelmini, and P. Gondolo, J. Cosmol. Astropart. Phys. 11 (2010) 028.

[12] M. Fairbairn and T. Schwetz, J. Cosmol. Astropart. Phys. 01 (2009) 037.

[13] C. Kelso and D. Hooper, J. Cosmol. Astropart. Phys. 02 (2011) 002.

[14] W. Seidel, WONDER 2010 Workshop, Laboratory Nazionali del Gran Sasso, Italy, 2010; IDM 2010 Workshop, Montpellier, France, 2010.

[15] J. Ellis, J. S. Hagelin, D. V. Nanopoulos, K. A. Olive, and M. Srednicki, Nucl. Phys. **B238**, 453 (1984).
[16] G. Jungman, M. Kamionkowski, and K. Griest, Phys. Rep. **267**, 195 (1996).
[17] G. Belanger, F. Boudjema, A. Pukhov, and R. K. Singh, J. High Energy Phys. 11 (2009) 026; Y. Akrami, P. Scott, J. Edsjo, J. Conrad, and L. Bergstrom, J. High Energy Phys. 04 (2010) 057.
[18] D. A. Vasquez, G. Belanger, C. Boehm, A. Pukhov, and J. Silk, Phys. Rev. D **82**, 115027 (2010).
[19] E. Kuflik, A. Pierce, and K. M. Zurek, Phys. Rev. D **81**, 111701 (2010); D. Feldman, Z. Liu, and P. Nath, Phys. Rev. D **81**, 117701 (2010).
[20] A. Bottino, N. Fornengo, and S. Scopel, Phys. Rev. D **67**, 063519 (2003); A. Bottino, F. Donato, N. Fornengo, and S. Scopel, Phys. Rev. D **78**, 083520 (2008); V. Niro, A. Bottino, N. Fornengo, and S. Scopel, Phys. Rev. D **80**, 095019 (2009); A. Bottino, F. Donato, N. Fornengo, and S. Scopel, Phys. Rev. D **72**, 083521 (2005); N. Fornengo, S. Scopel, and A. Bottino, Phys. Rev. D **83**, 015001 (2011); S. Scopel, S. Choi, N. Fornengo, and A. Bottino, arXiv:1102.4033 [Phys. Rev. D. (to be published)].
[21] V. Silveira and A. Zee, Phys. Lett. B **161**, 136 (1985).
[22] J. McDonald, Phys. Rev. D **50**, 3637 (1994).
[23] C. P. Burgess, M. Pospelov, and T. ter Veldhuis, Nucl. Phys. **B619**, 709 (2001).
[24] V. Barger, P. Langacker, M. McCaskey, M. J. Ramsey-Musolf, and G. Shaughnessy, Phys. Rev. D **77**, 035005 (2008).
[25] M. Gonderinger, Y. Li, H. Patel, and M. J. Ramsey-Musolf, J. High Energy Phys. 01 (2010) 053.
[26] X. G. He, T. Li, X. Q. Li, J. Tandean, and H. C. Tsai, Phys. Rev. D **79**, 023521 (2009); Y. Cai, X. G. He, and B. Ren, Phys. Rev. D **83**, 083524 (2011); M. Asano and R. Kitano, Phys. Rev. D **81**, 054506 (2010).
[27] J. Angle *et al.* (XENON Collaboration), Phys. Rev. Lett. **100**, 021303 (2008).
[28] Z. Ahmed *et al.* (CDMS Collaboration), Phys. Rev. Lett. **102**, 011301 (2009); Z. Ahmed *et al.* (CDMS Collaboration), Science **327**, 1619 (2010).
[29] C. Arina and M. H. G. Tytgat, J. Cosmol. Astropart. Phys. 01 (2011) 011.
[30] R. W. Schnee *et al.* (The SuperCDMS Collaboration), arXiv:astro-ph/0502435.
[31] E. Aprile (Xenon Collaboration), J. Phys. Conf. Ser. **203**, 012005 (2010).
[32] A. Abada and S. Nasri (work in progress).
[33] K. Nakamura *et al.* (Particle Data Group), J. Phys. G **37**, 075021 (2010).
[34] The effect of η_0 in the one-real-scalar extension of the standard model is discussed in D. N. Spergel and P. J. Steinhardt, Phys. Rev. Lett. **84**, 3760 (2000). See also [7].
[35] E. W. Kolb and M. S. Turner, *The Early Universe* (Addison-Wesley, Reading, MA, 1998).
[36] E. Komatsu *et al.*, Astrophys. J. Suppl. Ser. **192**, 18 (2011).
[37] S. Weinberg, *Cosmology* (Oxford University Press, 2008).
[38] R. Gaitskell, V. Mandic, and J. Filippini, SUSY Dark Matter/Interactive Direct Detection Limit Plotter, http://dmtools.berkeley.edu/limitplots.